Diffusion kinetics of molecular probe in thin poly(vinyl alcohol)-based films

Majerczak, Katarzyna; Shi, Zhiwei; Zhang, Zhanping; Zhang, Zhenyu Jason

DOI:
10.1016/j.porgcoat.2023.107833

Document Version
Publisher's PDF, also known as Version of record

Citation for published version (Harvard):
Majerczak, K, Shi, Z, Zhang, Z & Zhang, ZJ 2023, 'Diffusion kinetics of molecular probe in thin poly(vinyl alcohol)-based films', *Progress in Organic Coatings*, vol. 185, 107833.
https://doi.org/10.1016/j.porgcoat.2023.107833

Progress in Organic Coatings 185 (2023) 107833

Contents lists available at ScienceDirect

Progress in Organic Coatings

journal homepage: www.elsevier.com/locate/porgcoat

Diffusion kinetics of molecular probe in thin poly(vinyl alcohol)-based films

Katarzyna Majerczak [a], Zhiwei Shi [b], Zhanping Zhang [b], Zhenyu Jason Zhang [a,*]

[a] School of Chemical Engineering, University of Birmingham, Edgbaston, B15 2TT Birmingham, United Kingdom
[b] The Procter and Gamble Company, Mason Business Center, 8700 Mason-Montgomery Road, Mason, OH 45040, United States

ARTICLE INFO

Keywords:
Migration
FRAP
AFM
PVA
Thin film

ABSTRACT

We investigated the diffusion characteristics of a molecular probe in organic films of poly(vinyl alcohol) (PVA) that replicate formulations used as packaging materials. Diffusion kinetics of Rhodamine B (RhB) was measured in thin films of PVA containing glycerol and surfactants of various headgroup chemistry (cationic/nonionic/anionic) using fluorescence recovery after photobleaching and atomic force microscopy. Here we show how diffusion is determined by both molecular arrangement within the film and the nature/magnitude of intermolecular interactions. Addition of glycerol could improve the flexibility of PVA chains initially but imposed steric inhibition once the concentration exceeded the threshold of 44 wt%. In all investigated formulations, RhB exhibited diffusion-coupled mechanism. The presence of surfactants (at 6 wt%) reduced the diffusivity of RhB in PVA matrix for all types of surfactants used (by 30 %, 61 %, and 88 % for cationic, nonionic, and anionic surfactant addition compared to control sample, respectively). We conclude that steric inhibition effects underpin the diffusion of RhB in PVA thin films doped with nonionic surfactant. However, for PVA films with the addition of cationic or anionic surfactant, interactions between surfactant and fluorophore are likely responsible for the change in diffusivity of the molecular probe.

1. Introduction

Polymers are versatile materials used in many formulated products due to their strength, inertness, and low cost of production [1]. However, glassy polymers suffer from brittleness [2] and low flexibility [3], therefore commercial products must use formulations of polymer and several property-enhancing additives (e.g. plasticisers or reinforcements) [1]. While mechanical properties of the material are improved, the presence of additives in such complex matrix could lead to substantial issues due to molecular migration such as product degradation and release of toxic additives into the adjacent medium (e.g. atmosphere or food) [2–4]. Therefore, there is a pressing need to predict the behaviour of molecules within a particular system to minimise harmful influence of migration on the overall properties of the formulated products.

The complexity of molecular migration within polymer formulations primarily arises due to the wide variety of chemical environments that can be exhibited by each component. Among the many factors that influence this phenomenon are:

- the nature of the polymer (e.g. density, molecular weight (M_w) distribution [5], crystallinity, degree of crosslinking or branching, solubility, glass transition temperature, melting temperature, surface tension);
- the nature of the additives (e.g. size [6,7], shape [6,8,9], solubility [10], concentration [9], tendency to form micelles and lamellae);
- polymer-additive interactions [10] (e.g. through charge-charge interaction);
- overall compatibility [11];
- processing conditions (e.g. temperature, humidity) [12–14].

Molecular migration mechanisms (e.g. diffusion, shear stresses on the film, or spontaneous surface segregation) are driven by the balance between loss of translational entropy and gain in surface energy of the polymer matrix, leading to the formation of distinctive morphological features [15]. When considering an individual migration mechanism, movement of the guest molecules present in the system can be predicted. However, notwithstanding recent advances in polymer science, it remains challenging to fully predict the main mechanism of migration for any multi-component matrix either theoretically or computationally. Theoretical investigation (e.g. through statistical thermodynamics

* Corresponding author.
E-mail address: z.j.zhang@bham.ac.uk (Z.J. Zhang).

https://doi.org/10.1016/j.porgcoat.2023.107833
Received 1 May 2023; Received in revised form 9 July 2023; Accepted 25 July 2023
Available online 21 August 2023

methods such as Flory-Huggins theory) [16,17] of such systems is quite intricate as even though models can be used to describe bulk mixing between two chemically different species, they cannot be applied to the systems where local segregation close to the polymer/atmosphere interface takes place [15]. Therefore, they are inappropriate for modelling many real-world industrial formulations (e.g. polymer films doped with a surfactant) that exhibit the tendency for non-uniform distribution of the additive (e.g. the creation of a surfactant wetting layer) both at the air-film [18,19] and air-water interface [20,21] due to incompatibility between the species [18,22,23]. Moreover, the characteristics of mesostructures formed in these products is dependent on specific intermolecular interactions [21] that also need to be considered to provide a possible set of design criteria, which could minimise guest molecule migration in the polymer matrix while ensuring optimum distribution of additives [10,23].

A common approach to make these complex systems experimentally manageable is by using individual additive simulants rather than several additives that are used in real-life polymer formulations [24]. Consequently, current research focuses on two-component [25] or three-component systems [26]. While there is an in-depth understanding of interfacial phenomena in polymer blends [27] (including wetting layer formation) [28], it needs to be extended to molecular migration in multi-component systems as opposed to simpler formulations. Furthermore, while many studies have been carried out to explain the diffusion of molecules from polymer films to surrounding media [29–33], fewer describe migration in the opposite direction [34].

Thin films of poly(vinyl alcohol) (PVA) are of particular interest due to their wide industrial application such as water soluble packaging materials in fast moving consumer goods. They are formulated with several additives such as surfactants and plasticisers to improve film forming properties and are in direct contact with chemical products - usually concentrated surfactant solutions. Over time, small molecules from the product would migrate into the PVA matrix, leading to a heterogeneous distribution of additives within the packaging film and reduced shelf-life of the product. By mimicking migration towards the packaging film – e.g. by studying three component polymer/plasticiser/surfactant, rather than two component polymer/plasticiser or polymer/surfactant systems – prediction of more complex migration behaviour will become possible.

Techniques used for migration measurements can establish rapid diffusion coefficients (i.e. 10^{-8}–10^{-5} cm^2/s, corresponding to the movement of single molecules or submicron-sized particles in low viscosity liquids) [35], as well as slow diffusion processes (i.e. 10^{-12}–10^{-8} cm^2/s, corresponding to the movement of particles in solids) [35]. Raman correlation spectroscopy [36], photon correlation spectroscopy [37], fluorescence correlation spectroscopy (FCS) [38–40], magnetic resonance imaging [41,42] or capillary flow [43] are exemplary techniques from the first group, while nuclear magnetic resonance spectroscopy [44], holographic relaxation spectroscopy [45], ion beam analysis [46,47], and fluorescence recovery after photobleaching (FRAP) [48]. Among these, FRAP is one of the most well-established methods [49] that allows control over the time scales of the measurements by varying the size of the bleached region [35]. FRAP has been successfully applied to various systems – from polymer films (also below their glass transition, T_g) [50] through multilayer systems [51] to biological samples [52] – enabling direct detection of molecular diffusion within a complex film, calculation of fraction of immobile molecules, and investigation into the dominant migration mechanisms present.

This work uses FRAP and atomic force microscopy (AFM) to investigate the diffusion kinetics of Rhodamine B (RhB) through PVA-based thin films. This molecular probe was chosen due to its wide industrial applications – it is present in paints, leather, paper and textile industry for printing and dyeing [53–55] – and its wide usage in studies of molecular migration [56], including in PVA [57]. The diffusion kinetics was recorded as a function of additive concentration (plasticiser) and guest molecule presence (surfactants of various headgroup chemistry) in thin (ca. 100 nm) PVA films. Investigation of thin films together with relatively low numerical aperture of the objective leads to bleaching without noticeable gradient in z-direction, hence enabling investigation of lateral diffusion only [58]. Establishing migration phenomena on the nanoscale in chosen system should therefore enable identification of key factors that influence molecular migration in formulated products displaying preferential segregation at the interface [23] and provide answers for problems faced in multicomponent formulations.

2. Materials and methods

2.1. Materials

Poly(vinyl alcohol) (PVA, Sigma-Aldrich P8136, M_w = 30–70 kg/mol, degree of hydrolysis (DH) = 87–90 %), glycerol (Sigma-Aldrich G9012, ≥99.5 %), sodium dodecyl sulfate (SDS, Fisher Scientific S/5200/53), decaethylene glycol monododecyl ether ($C_{12}E_{10}$, Sigma-Aldrich P9769), cetyltrimethylammonium bromide (CTAB, Sigma-Aldrich H5882, ≥98 %), rhodamine B (RhB, Sigma-Aldrich R6626, ≥95 %, HPLC), and HPLC water (HPLC Plus, Sigma Aldrich 34877-M) were purchased and used as received.

2.2. Solutions preparation

PVA was dissolved in HPLC water by heating up to 75 °C with continuous stirring (for ca. 2 h or until completely dissolved) to obtain 4 % (w/v) PVA solution and subsequently cooled to room temperature. Solutions of 4 % (w/v) glycerol, 1 % (w/v) SDS, and 1 % (w/v) CTAB were prepared by dissolving required amount of substance in HPLC water and stirring at room temperature for ca. 4 h. Aqueous solutions of 1 % (w/v) $C_{12}E_{10}$ were prepared at 30 °C with continuous mixing for ca. 2 h and subsequently cooled to room temperature.

Solutions of RhB were prepared by dissolving tracer in solution containing desired polymer/plasticiser/surfactant volume ratio created by mixing stock solutions and stirring overnight with protection from the light made of aluminium foil. Solutions with the addition of surfactant were heated up to 50 °C for 15 min to avoid formation of surfactant mesophases. All investigated samples were sonicated for 20 min at ca. 30 °C (sonication power 180 W), and cooled down to room temperature before use.

2.3. PVA thin film preparation

Thin (ca. 100 nm) PVA films were prepared by spin casting 200 µl of PVA solution onto glass slide using a spin coater (Spin 150i, SPS-Europe) with the spin speed of 2000 rpm for 100 s. Glass slides (1 in. squared) were cleaned using piranha solution [59], followed by sonication (three times, 10 min each sonication) in ultrapure deionized water (Mili-Q, 18.2 mΩ cm) and drying by nitrogen. Thin PVA films on glass substrates were placed facing down on cleaned cover slips (cleaned following the same procedure) with silicone spacer (thickness 0.45 mm). For films prepared from filtered solutions, mixtures made as described above were then filtered through a syringe filter (0.22 µm pore size) to remove any aggregates, followed by spin coating.

2.4. Diffusion measurements

FRAP experiments were performed using a confocal microscope (ZEISS LSM 780) under a 10× water immersion objective. To excite the fluorophore, 488 nm line of the Ar laser was used at 1.5 % of its maximum power for image acquisition and at maximum power for bleaching.

The radius of the bleach spot was set to 3 µm, with the image size equal to 60.7 µm square. Because the resulting radius after bleaching differed from nominal radius, diffusion coefficient was calculated using formula valid for samples that can be treated as 2D objects [60]:

$$D_{FRAP} = \frac{r_n^2 + r_e^2}{8\tau_{1/2}} \quad (1)$$

where D_{FRAP} is the effective diffusion coefficient of the fluorophore in the thin film, r_n is the nominal radius for the experiment, r_e is the resulting radius post bleaching, and $\tau_{1/2}$is the half recovery time. Resulting radius was calculated using fluorescence intensity profiles following a published method [60]. Intensity profiles prior and post photobleaching were extracted using ImageJ programme. Bleaching was repeated until fluorescence intensity was reduced to <70 % of the initial signal. For some positions on the samples, diffusion was too quick and the bleaching was not possible, which are denoted as positions with no possible bleaching.

To take into consideration the heterogeneous distribution of the fluorophore within the PVA film as well as possible intensity changes during imaging, a normalisation procedure for calculating the $\tau_{1/2}$ was performed. Except of the bleached region, fluorescence intensity was measured at the corners of the captured image (positions 2–5, Fig. S1 in Supporting Information). Normalised intensity was calculated using formula:

$$I_N = \frac{I_1}{I_{2-5}} \bullet \frac{I_{2-5(b)}}{I_{1(b)}} \quad (2)$$

where I_1 and $I_{1(b)}$ are intensity signals in the bleached region at a given time and the average value from three measurements at bleached region prior to bleaching, I_2-I_5 and $I_{2(b)}$-$I_{5(b)}$ are the average intensity values from positions 2–5 at a given time and prior to bleaching as the average from three measurements, respectively. The normalised fluorescence intensity was then used to calculate the $\tau_{1/2}$.

For each composition, three PVA thin films prepared from at least two different stock solutions were analysed. Due to the non-uniform nature of the surface for majority of the samples (Table S1), 10 positions from each sample were investigated, resulting in 30 total diffusion coefficient values unless stated otherwise. For samples prepared from filtered solution, one PVA-based film was prepared, on which 10 positions were investigated.

2.5. Surface morphology measurement

Thin films for AFM measurements were prepared both with the addition of RhB (the same way as samples used for FRAP analysis) and without the fluorophore (films spin coated from the solutions without RhB of desired polymer/plasticiser/surfactant ratio) as described above. AFM measurements were performed on a Dimension 3100 AFM (Veeco) using cantilevers of spring constant of around 40 N·m^{-1} (μmasch, HQ: NSC15/AL BS, aluminium coating). Morphology and thickness changes as a function of changes in film composition were investigated. The latter was assessed by performing scratch test and applying voltage difference of 14 V to scratch the film surface using AFM tip at scanning angle equal to 0°. The scratch was subsequently imaged at the scanning angle equal to 90° (perpendicular to the created scratch). For each sample, three scratches were made and at least three profiles from each scratch were extracted. The sample thickness was taken as the average value from the analysed positions.

3. Results and discussion

3.1. Effect of glycerol concentration on the diffusion of RhB in PVA films

Glycerol present in PVA matrix acts as a plasticiser, replacing PVA-PVA hydrogen bonds with PVA-glycerol bonds. Consequently, an increase in PVA chain mobility and free volume [61] is noted. Changes in intermolecular interactions result in variations in thermal properties of the plasticised polymer formulations. For example, a decrease in T_g for the formulations with increasing glycerol concentration is observed (from 53.3 °C to 26.8 °C for pure PVA of the same DH and M_w as polymer used in this study and PVA/20 wt% glycerol formulation, respectively) [62], with T_g behaviour with increasing plasticiser concentration showing a good agreement with Gordon-Taylor equation [63]. These changes result in structural changes of plasticised polymer matrix, including a decrease in the degree of crystallinity [63,64] and the apparent crystallite size in the PVA samples (from 2.4 nm vs 2.2 nm for pure PVA and PVA/20 wt% glycerol formulation, respectively) [62].All of these factors affect the diffusion rate of guest molecules in the system. To investigate the influence of glycerol on diffusion of the tracer, samples of different plasticiser content in thin films were prepared (Table 1).

PVA samples containing up to 75 % of glycerol all produced films of uniform thickness (Table 1). Despite changes in glycerol content, no noticeable change in PVA film morphology was observed – a characteristic roughness of ca. 0.4 nm was present for all investigated glycerol concentrations (Fig. 1), which suggests that the plasticiser was uniformly distributed in the PVA matrix [23]. However, increased glycerol concentration led to a decreased viscosity of PVA solution [65] hence PVA films with reduced thickness. In the absence of a polymer matrix to structure the film, it was impossible to reliably determine the thickness of films with composition G. Further, addition of RhB did not seem to change PVA film surface morphology.

Not only film thickness, but also RhB diffusion in the PVA film showed significant dependence on plasticiser content (Fig. 2). The diffusion rate of RhD in the benchmark, pure PVA films, was equal to 0.231 μm^2·s^{-1} but increased to 0.589 and 0.712 μm^2·s^{-1} in compositions PVA16.7 and PVA25, respectively. This trend varied for higher glycerol concentrations as after initial increase in diffusivity, the diffusion coefficient decreased drastically to 0.090 and 0.082 μm^2·s^{-1} for samples PVA50 and PVA75, followed by slight increase in tracer diffusion coefficient (0.215 μm^2/s, Fig. 2) in films prepared from pure glycerol solution. The diffusion data acquired shows a similar trend to that in a previous work concerning diffusion in thick PVA-glycerol films of 30–50 μm thickness [35] (cf. 80–140 nm), whereby significant increase in RhB diffusion coefficient was observed upon addition of glycerol (0 to 40 wt %), increasing from 10^{-5} to 10^{-1} μm^2·s^{-1}.

The discrepancy in the absolute diffusion coefficient values reported between the two studies may be attributed to the different preparation methods and PVA film thickness: the effect of interface (polymer-air and polymer-substrate) plays a critical role for thin PVA film, but could be negligible for the thick counterpart [66,67]. As a consequence, properties of thin films vary compared to their thicker equivalents. While the methodology applied here can model diffusion as a 2D process, similar assumptions are not valid for thick films where bleaching and diffusion take place not only at the surface, but also at the layers below the surface. Moreover, thick films are more prone to water absorption due to the higher weight of glycerol present in the matrix compared to thin counterpart. Due to its hydrophilic nature, glycerol increases water

Table 1
Compositions and thickness of all thin films investigated in the present work. Calculations of the glycerol content in the films do not include water present in the films. P, G, and S refer to PVA, glycerol, and surfactant, respectively. Due to high non-uniformity and poor film-forming properties of glycerol, scratch test was not performed on these samples.

Sample	S used	Molar ratio (P:G:S)	G conc. (wt %)	Thickness (nm)
PVA	–	1:0:0	0	140 ± 3
PVA16.7	–	1:109:0	16.7	136 ± 5
PVA25	–	1:181:0	25.0	116 ± 4
PVA50	–	1:543:0	50.0	102 ± 3
PVA75	–	1:1629:0	75.0	79 ± 3
G	–	0:1:0	100	–
PVA-SDS	SDS (−)	1:181:14	23.5	29 ± 4
PVA-$C_{12}E_{10}$	$C_{12}E_{10}$ (0)	1:181:7	23.5	99 ± 1
PVA-CTAB	CTAB (+)	1:181:11	23.5	84 ± 17

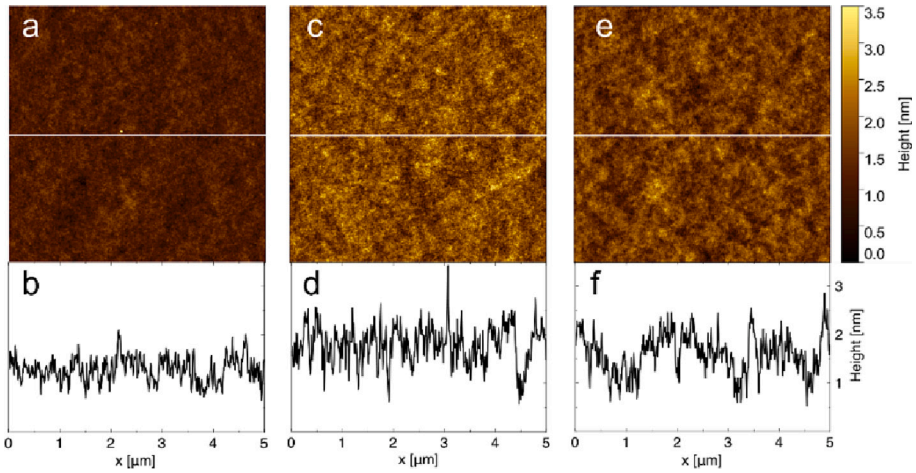

Fig. 1. Morphology and corresponding sectional height profile of compositions (a,b) PVA, (c,d) PVA25, and (e,f) PVA50 investigated acquired by AFM.

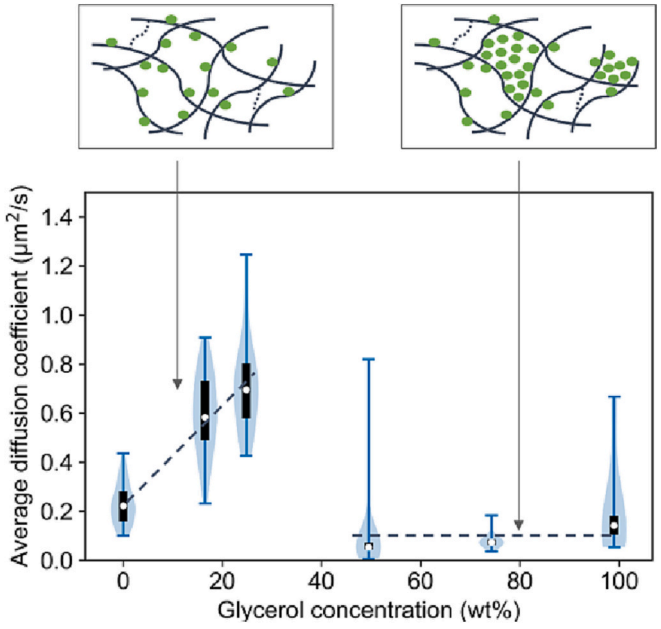

Fig. 2. Diffusion coefficients of RhB in PVA thin films. White circles show median values, black rectangles represent interquartile range (25–75 %), while blue lines - the entire range of recorded values. The shaded area (violin shape) is the estimated diffusion coefficient distribution, according to the kernel density estimation algorithm. In the schematic diagrams, lines represent individual PVA chains, dashed lines - PVA-PVA bonding, while green circles represent glycerol. Dashed lines on the graph represent approximate trend of RhB diffusion coefficient changes with increasing glycerol concentration. (For interpretation of the references to colour in this figure legend, the reader is referred to the web version of this article.)

sorption in hydrophilic polymer films, leading to an increased diffusion coefficient up to 2 orders of magnitude compared to pure polymer matrices [68].

It is worth noting that RhB was not distributed evenly in all PVA thin films studied, evidenced by variation in the background intensity (Table S1 in Supporting Information) also visible for other fluorophores (Fig. S2 in Supporting Information). With an increasing glycerol concentration, the number of regions of higher intensity increased while the averaged background intensity decreased. This led to a dependence of RhB diffusion coefficient on measurement position, and consequently a higher standard error for samples PVA50 and PVA75 (Fig. 2). It shows that an increasing glycerol fraction results in heterogenous molecular distribution within the PVA film, with RhB aggregation expected to occur in regions of high glycerol concentration. The observed sudden reduction in diffusivity is likely a consequence of reaching PVA-glycerol compatibility limit [61,69]. Previous study showed that glycerol and partially hydrolysed PVA are compatible up to 39 wt% glycerol content [61], which is in good agreement with our results (Fig. 2). Before reaching compatibility limit, addition of glycerol leads to increase in free volume of the film and mobility of the fluorescent tracer therein. However, further addition of plasticiser results in increased impact on chain separation leading to phase separation in the films [69] and formation of glycerol- or PVA-rich regions. Consequently, the diffusion coefficient of RhB decreases due to the formation of interfaces between the two phases and resultant barriers for RhB to diffuse across these boundaries. Additionally, in the PVA-rich phase lack of plasticisation with glycerol decreases diffusion rates. Regions of high value of diffusion coefficient are likely of similar local compositions to that of sample PVA16.7 or PVA25.

The effect of glycerol (plasticisation) is also evidenced by the number of positions with immobile molecules during FRAP analysis, signified by a lower equilibrium fluorescence signal post bleaching than prior to bleaching. For the pure PVA film, nearly all investigated positions had some portion of immobile molecules. However, much fewer positions in PVA films had immobile molecules upon addition of glycerol below compatibility limit (Table 2). For PVA films above the compatibility limit, the overall increase in average fraction of immobile molecules compared to pure PVA was reported.

The value of the diffusion coefficient depends on both nominal and actual bleach radii in addition to $\tau_{1/2}$ values (Eq. (1)). Therefore, $\tau_{1/2}$ and diffusion coefficient do not necessarily show inversely proportional character of changes with an increasing glycerol content. Indeed, while

Table 2
Immobile molecules data and bleaching data for samples A-F.

Composition	Positions with immobile molecules	Average fraction of immobile molecules	Positions with no possible bleaching
PVA	25	$1.73{\cdot}10^{-2} \pm 2.3{\cdot}10^{-5}$	0
PVA16.7	3	$1.48{\cdot}10^{-2} \pm 7.3{\cdot}10^{-3}$	0
PVA25	4	$5.7{\cdot}10^{-3} \pm 1.3{\cdot}10^{-3}$	1
PVA50	9	$5.4{\cdot}10^{-2} \pm 2.4{\cdot}10^{-2}$	0
PVA75	6	$2.1{\cdot}10^{-2} \pm 7.2{\cdot}10^{-3}$	1
G	5	$1.3{\cdot}10^{-1} \pm 4.0{\cdot}10^{-2}$	24
PVA-SDS	7	$9.7{\cdot}10^{-2} \pm 2.4{\cdot}10^{-2}$	4
PVA-$C_{12}E_{10}$	5	$7.4{\cdot}10^{-2} \pm 2.0{\cdot}10^{-2}$	0
PVA-CTAB	5	$4.4{\cdot}10^{-2} \pm 1.3{\cdot}10^{-2}$	5

for formulations of up to 50 wt% glycerol, the trend of average $\tau_{1/2}$ change with glycerol concentration was reversed compared to that of diffusion coefficient - initial decrease for PVA16.7 and PVA25 samples followed by increase between glycerol concentrations of 25 and 50 wt%, Table 3 (vide infra) - for PVA75 sample again a small decrease of $\tau_{1/2}$ values was noted. The actual bleach radius decreased with increasing glycerol concentration (Table S2 in Supporting Information), which explains the difference in $\tau_{1/2}$ values for PVA50 and PVA75 samples (less time required for recovery due to decreased bleach size) despite the similar values of diffusion coefficient.

Sample G (pure glycerol) showed a particularly high dependence on analysis area, with many positions recording no possible bleaching due to too fast diffusion of RhB (values not included in average diffusion coefficient calculations, Table 2). A distinctively different recovery profile, in comparison with PVA film, was observed in the few regions where FRAP measurements were possible: after initial increase of normalised intensity and reaching >50 % of the recovery, a decreased fluorescence signal was observed (Fig. 3a). Non-uniform morphology and poor film-forming properties of glycerol may be responsible for this unexpected behaviour observed after reaching half recovery.

AFM images show that RhB is located in glycerol domains creating characteristic pattern on the surface on a similar length scale to the bleached spot size (Fig. 3b, Fig. S3 in Supporting Information) and indicate that the measured diffusion takes place within a single glycerol domain or a few small ones. Hence, positions in which RhB showed a slow diffusion coefficient may be a consequence of diffusion between small glycerol domains, while very fast diffusion or not possible bleaching - within single domain. FRAP measurements on the pure glycerol films can therefore be useful in interpreting the behaviour of the PVA-based thin films that exhibited heterogeneity. For instance, single positions with no possible bleaching for samples of composition PVA25 and PVA75 (Table 2) suggest creation of nano-domains rich in glycerol and fast diffusion within these regions in otherwise uniform polymer films.

Overall, plasticiser has a complex impact on tracer diffusion within the system. At low glycerol concentration further plasticiser addition promotes faster RhB diffusion, however, diffusion is significantly reduced once the compatibility limit of glycerol and PVA is reached. At the extreme of diffusion through pure plasticiser, precise diffusion measurement is hampered by the poor film-forming behaviour of glycerol. These characteristic behaviours for different film compositions can be further investigated by analysing not just the measured rate of RhB diffusion, but also the shape of the curve to determine the recovery mechanism.

3.2. Diffusion mechanisms in thin PVA films

The reduction in the diffusion coefficient above the glycerol-PVA compatibility threshold is accompanied by the changed characteristics of the fluorescence recovery profile. This can be seen in Fig. 4a and Fig. 4b, which show the normalised recovery curves for sample PVA25 and PVA50 – below and above PVA-glycerol compatibility threshold, respectively.

Table 3
Half recovery times for different bleach radii as a function of film composition.

Composition	Average $\tau_{1/2}$ for bleach size 3 μm (s)	Range of $\tau_{1/2}$ for bleach size 3 μm (s)	$\tau_{1/2}$ for bleach size 5.1 μm (s)	Expected diffusion mechanism
PVA	19.71 ± 0.86	12.43–33.75	24.43; 26.11	Diffusion-uncoupled
PVA16.7	6.26 ± 0.19	4.28–8.48	6.10; 11.24	Diffusion-coupled
PVA25	5.31 ± 0.17	3.89–7.83	7.56;17.80	Diffusion-coupled
PVA50	57.15 ± 3.18	5.54–85.48	24.35; 102.34	Diffusion-coupled
PVA75	34.03 ± 1.67	19.87–62.22	47.40; 88.30	Diffusion-coupled

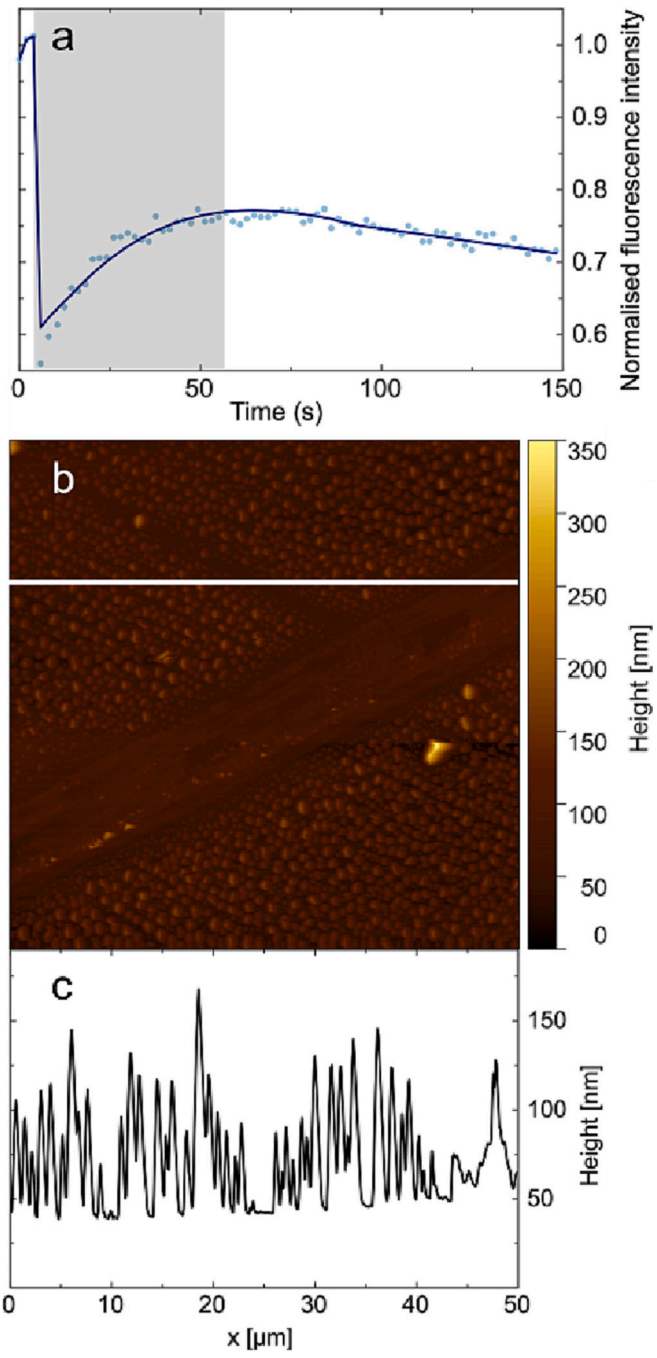

Fig. 3. (a) FRAP recovery curve for representative position for pure glycerol sample (shaded area represents half recovery time), (b) AFM image and (c) the corresponding surface profile of pure glycerol sample (scratch region).

When glycerol concentration was equal or below 25 wt%, fluorescence recovery occurred in two distinct stages: the initial bleaching was followed immediately by a sharp recovery in fluorescence intensity, after which the sample slowly reached equilibrium (Fig. 4a). For PVA films with glycerol concentration >50 wt%, the fluorescence signal reached equilibrium at a constant rate (Fig. 4b) without the initial fast recovery. Consequently, $\tau_{1/2}$ became longer, and resulted in lower calculated diffusion coefficient of the fluorophore.

Changes in the recovery curves suggest that different mechanisms are responsible for the observed variations in diffusivity. Two

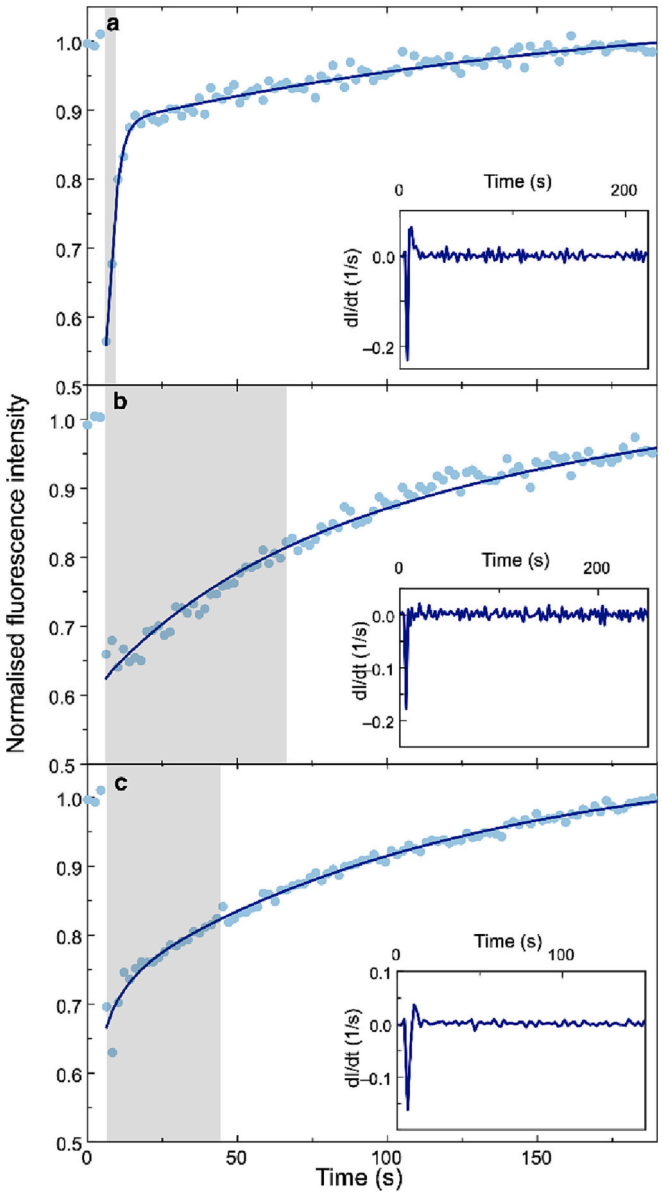

Fig. 4. Fluorescence recovery curve for samples of compositions (a) PVA25, (b) PVA50, and (c) PVA25 with increased bleach size. The insets present the derivative of fluorescence intensity over time, while shadowed regions represent half recovery time for given formulation.

fundamental processes occur during the fluorescence recovery: probe molecules diffuse through the film (unbleached fluorophores into the analysis region and bleached fluorophores out) and interact with neighbouring molecules via binding [70]. How these processes relate to one another results in differences in the measured recovery mechanism. The processes of diffusion and binding can either occur separately (diffusion-uncoupled mechanism), or at the same time (diffusion-coupled mechanism). By determining the mechanism of migration, it can be concluded whether the detected diffusion coefficient applies only to pure diffusion or to effective diffusion (diffusion combined with binding) of the tracer within the sample.

In the diffusion-uncoupled mechanism, the recovery curve could be divided into two sections. Shortly after photobleaching, tracer molecules rapidly diffuse into the bleached region driven by the concentration gradient and occupy available space. Binding only occurs once the diffusion is complete. The rate of recovery for this part of the curve corresponds to the nature and extent of the binding – the tighter the binding state, the slower the recovery [70]. In diffusion-coupled recovery, diffusion and binding are indistinguishable due to similar time scales of these mechanisms [70]. They occur together – individual particles migrate then replace bleached molecules with fluorescent molecules – until the equilibrium is reached.

Because diffusion is dependent on the radius of photobleaching, while binding kinetics are not, the diffusion mechanism can be determined by performing measurements on two different bleach sizes. Diffusion-coupled recovery shows different $\tau_{1/2}$ values for different bleach radius on the same sample (as diffusion in these samples is gradual), while for diffusion-uncoupled recovery they remain the same within experimental error [70]. As full recovery did not take place in all investigated samples and second bleaching at the same position was proven to have different kinetics compared to the first [71], the measurements of recovery within increased bleach size were performed at different positions. Given the large range of absolute $\tau_{1/2}$ values recorded during initial 3 μm bleaching experiments, experiments on a larger (5.1 μm size) bleach size were compared against the absolute values of RhB recovery $\tau_{1/2}$ rather than the average value (Table 3). This way, it was possible to establish the diffusion mechanism for all samples except the pure glycerol (sample G), due to the aforementioned non-uniformity of these samples.

Although recovery curves acquired from samples PVA16.7 and PVA25 initially suggest a diffusion-uncoupled mechanism, the range of RhB $\tau_{1/2}$ recorded at the larger spot size had a higher upper limit than the 3 μm spot, suggesting a shift of the distribution to higher values. Moreover, the shape of the recovery curve changed with the increasing bleach size: the initial fast recovery regime was less pronounced comparing to that acquired with 3 μm bleach size (Fig. 4c cf. Fig. 4a), which suggests a diffusion-coupled mechanism. The only exception was sample of pure PVA without glycerol, where $\tau_{1/2}$ values overlapped completely between both bleach sizes, indicating diffusion-uncoupled mechanism. However, due to the wide distribution of absolute $\tau_{1/2}$ values, there is a possibility that the diffusion kinetics are diffusion-coupled and recorded values of $\tau_{1/2}$ for increased bleach radius are in the lower end of the shifted distribution of $\tau_{1/2}$ for smaller bleach size. Therefore, the FRAP results acquired from all samples were analysed using diffusion-coupled mechanism, with calculated diffusion coefficient representing the effective diffusivity (i.e. describing all mechanisms that influence migration in these systems).

3.3. Modelling molecular diffusion in thin PVA films

To further investigate changes in the acquired diffusion kinetics with film composition despite all PVA-based thin films assumed to follow diffusion-coupled mechanism, the FRAP recovery curves were treated as the sum of two exponentials representing fast and slow migrating species present in the system. The parameters for effective diffusion of each component in the system can be modelled using the equation below [72]:

$$I_N = I_{N(b)} - I_{N,fast} \bullet exp\left(-\frac{t}{T_{fast}}\right) - I_{N,slow} \bullet exp\left(-\frac{t}{T_{slow}}\right) \quad (3)$$

where I_N and $I_{N(b)}$ are the normalised (following Eq. 2) intensities of the recovery curve at a given time t and at the beginning of experiment, respectively; $I_{N,fast}$ and $I_{N,slow}$ are normalised amplitudes of the fast and slow migrating molecule fractions (correlated with their fractional concentration) after photobleaching. Using fitted parameters T_{fast} and T_{slow}, the values of $\tau_{1/2}$ for a given kind of molecule can be calculated as [73]:

$$\tau_{1/2_x} = ln(0.5) \bullet T_x \quad (4)$$

where T_x is either T_{fast} or T_{slow}, and $\tau_{1/2x}$ is the half recovery time for the respective molecules. Although Eq. (3) cannot be used to accurately calculate the magnitude and number of binding interactions for

diffusion-coupled recovery [70], it can be applied to evaluate the diffusion kinetics of the two species, as presented in Table 4.

The satisfactory fit of FRAP recovery data to Eq. (3) (Fig. 4a, Fig. 4b) suggests that there are three kind of species present in discussed system [68]:

- Fast migrating molecules, with low value of $\tau_{1/2}$ likely exhibiting weak physicochemical interactions between the tracer and PVA/glycerol matrix.
- Slow migrating molecules that can not only interact in a similar way to fast population, but also are more prone to binding effects and steric hindrance effects.
- Entirely immobile molecules over the time scale of experiment.

The average values of $\tau_{1/2}$ for fast and slow migrating molecules are clearly dependent on the amount of glycerol in the PVA films, with $\tau_{1/2}$ for both species showing a similar behaviour to that of $\tau_{1/2}$ assuming only one kind of migrating species for 3 μm bleach size (Table 3) - initial decrease below the PVA-glycerol compatibility limit, followed by an increase (Table 4). However, the ratio between normalised amplitude of fast and slow molecules shows a different trend. Specifically, its value initially increases between pure PVA samples and PVA16.7 samples (ratio equal to 1.55 and 2.93, respectively) and then decreases for PVA25 sample (equal to 1.58) despite higher diffusion coefficient values reported in Fig. 2 for formulation C. We suggest that the variations in the normalised amplitudes for slow and fast migrating molecules and their respective $\tau_{1/2}$ are responsible for variations in overall kinetic behaviour of RhB in investigated formulations. Between the compositions PVA16.7 and PVA25, the decrease in diffusion times with increasing glycerol concentration has more profound effect than decreasing amplitude of fast migrating molecules, resulting in overall increasing effective diffusion coefficient. Upon increasing glycerol concentration above PVA-glycerol compatibility limit, increasing diffusion times for both fast and slow migrating species and decreased ratio of amplitude between fast and slow migrating molecules result in change in overall diffusion kinetics (Fig. 4) and decrease in average diffusion coefficient. Similarly, for samples PVA50 and PVA75 variations in amplitude and $\tau_{1/2}$ for both migrating species balance out, leading to similar effective diffusion times after accounting for variations in the bleached spot size (Table S2 in Supporting Information).

3.4. Effect of surfactant of various headgroup chemistry addition

Previous studies show that high concentration of surfactants of various headgroup chemistry (cationic, nonionic and anionic) in plasticised PVA film can change its surface morphology and molecular arrangement within the matrix, with the magnitude of changes dependent on polymer-surfactant compatibility and surface energy of the surfactants [22,23]. These factors are also expected to dominate formulations of plasticised PVA with lower surfactant content. As size of the migrating tracer remains unchanged, by introducing molecules with various headgroup chemistry it was possible to investigate the role of intermolecular interactions on the diffusion coefficient of the molecular probe. Compositions of PVA films prepared from the same polymer/plasticiser/surfactant weight ratios but varied surfactant chemistry are presented in Table 1.

Fig. 5 shows that adding surfactant (at 6 wt%) to glycerol-plasticised PVA films results in overall reduced diffusivity of the tracer by 30, 61, and 88 % for cationic, nonionic, and anionic surfactant, respectively, compared to the benchmark, sample PVA25 (equivalent composition when not doped with surfactants). However, the measured diffusion rate is highly dependent on the position on the sample, suggesting surfactant blooming or phase separation in the PVA thin films. This is consistent with previous studies that have shown phase separation in surfactant-doped films, despite the substantially lower surfactant concentrations used here than in those studies [22,23]. As a result, the average value of the tracer diffusion coefficient does not provide full information about the properties of the surfactant-doped compositions; instead, they are represented by the distribution of the absolute recorded values of diffusion coefficient.

The most drastic changes in diffusivity were observed for systems with cationic and anionic surfactants, where positions of both substantially lower RhB diffusion coefficient cf. PVA25 composition and positions where bleaching was not possible were recorded. The latter appeared as the fluorescence recovery rate became faster than bleaching or the fluorophore re-absorbed [74], and in most cases was connected with regions of higher fluorescence intensity prior to bleaching. In general, distribution of the fluorophore does not substantially vary compared to PVA25 sample (Table S1 in Supporting Information). As number of positions where bleaching was not possible was the highest for pure glycerol films, it is expected that in samples containing SDS and CTAB, these regions correspond to high local concentration of the plasticiser. Regions with slow diffusion coefficient of the tracer, on the other hand, are likely attributed to the excessive amount of surfactants: RhB was proven to interact with SDS [56,75] and CTAB on the same level of magnitude [76] due to ionic interactions, although SDS-RhB interactions are expected to be more favourable than CTAB-RhB interactions due to steric hindrance effects [65].

The effect of such molecular interactions is evidenced by comparing surface morphology of the PVA films with and without RhB. For PVA/glycerol/SDS films, surfactant blooms are incorporated into the film structure (Fig. 6a and b). However, with the presence of RhB, the film morphology is similar to that of plasticised PVA films (Figs. 1, 6c, and d).

Table 4
Average $\tau_{1/2}$ and normalised amplitude for fast and slow migrating molecules for investigated samples.

Composition	$I_{N,fast}$	$\tau_{1/2,fast}$ (s)	$I_{N,slow}$	$\tau_{1/2,\ slow}$ (s)	$I_{N,fast}$ / $I_{N,slow}$
PVA	0.31 ± 0.01	15.05 ± 0.68	0.20 ± 0.01	166.88 ± 14.62	1.55 ± 0.01
PVA16.7	0.41 ± 0.01	5.47 ± 0.24	0.14 ± 0.01	151.90 ± 11.73	2.93 ± 0.02
PVA25	0.30 ± 0.01	3.67 ± 0.11	0.19 ± 0.01	115.04 ± 5.58	1.58 ± 0.01
PVA50	0.15 ± 0.02	42.00 ± 4.11	0.26 ± 0.02	201.15 ± 19.86	0.58 ± 0.04
PVA75	0.23 ± 0.01	23.96 ± 2.10	0.19 ± 0.02	288.29 ± 48.13	1.21 ± 0.03
PVA-SDS	0.13 ± 0.02	8.18 ± 1.43	0.25 ± 0.02	157.15 ± 15.33	0.52 ± 0.04
PVA-$C_{12}E_{10}$	0.14 ± 0.01	2.16 ± 0.34	0.31 ± 0.01	51.24 ± 4.17	0.45 ± 0.02
PVA-CTAB	0.23 ± 0.02	4.15 ± 0.99	0.23 ± 0.02	101.00 ± 14.13	1.00 ± 0.03

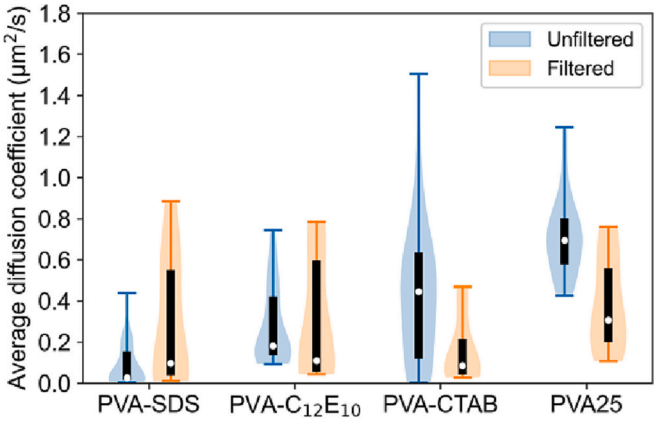

Fig. 5. Average diffusion coefficient and its distribution for surfactant-doped films prepared from filtered and non-filtered solutions.

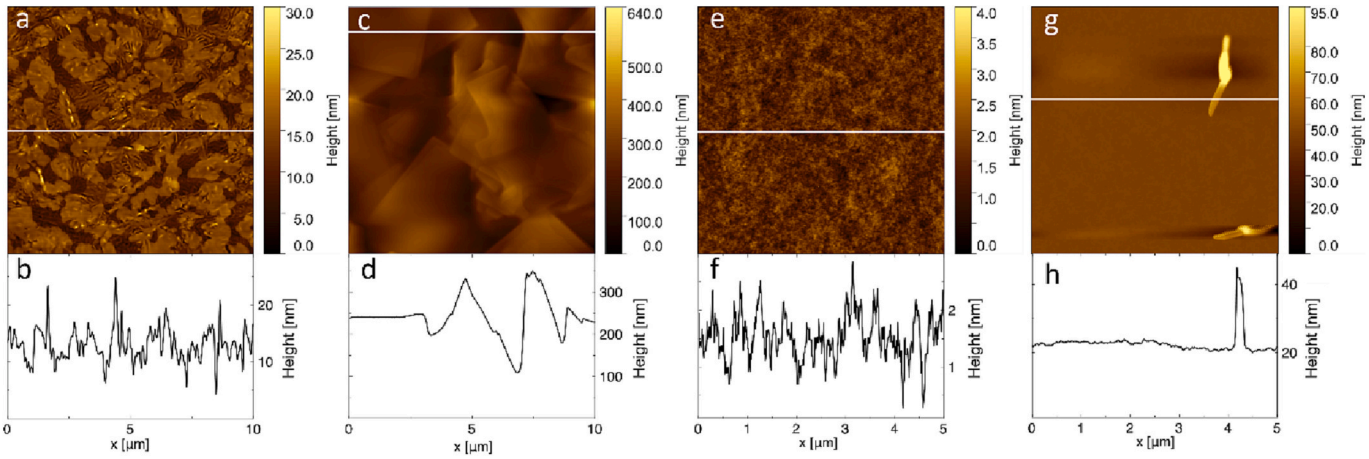

Fig. 6. Morphology and surface profiles of PVA-SDS sample (a,b) in the absence of RhB and (c,d) containing RhB; PVA-$C_{12}E_{10}$ sample doped with RhB: (e,f) background morphology and (g,h) surface features.

Moreover, prior to spin coating, small green precipitates believed to be crystals were observed after RhB was added into the solution used for film preparation, which is likely due to the electrostatic interactions between the anionic surfactant and the cationic functional groups of the RhB that form an active centre to accelerate nucleation of RhB precipitates [77]. However, a lower average diffusion coefficient compared to PVA25 sample was still recorded in the regions without precipitates (Fig. 5), suggesting that SDS and RhB are also present in PVA-glycerol matrix. AFM measurements on samples of different SDS content indicate that SDS concentration above 2 wt% changes the PVA film morphology on the preparation day [78] (not shown here, for brevity). In addition to morphology, SDS also changes PVA-glycerol interactions into SDS-glycerol interactions, resulting in creation of lamellae at higher surfactant concentrations [22]. This in turn results in lower degree of PVA plasticisation and consequent possible reduction of tracer diffusion coefficient. The sum of these factors – decelerated diffusion of RhB due to interactions with SDS present in the matrix and non-uniform morphology of PVA-SDS sample – can explain the strongest decrease in tracer diffusion coefficient observed upon introducing SDS into the system.

These findings are confirmed by scratch test results (Table 1). For samples doped with SDS, scratches were performed at positions without visible surface features, which shows a decrease in film thickness equal to 75 % compared to PVA25 film. The thickness of films containing $C_{12}E_{10}$ and CTAB also showed decreased thickness compared to PVA/glycerol films of the corresponding plasticiser concentration. For films with $C_{12}E_{10}$, this can be correlated with decrease in viscosity of the solutions used for film preparation [65]. For samples with CTAB, however, the decrease in film thickness is observed despite similar viscosity of the solution used for preparation of PVA-CTAB sample compared to PVA25 sample [65]. These trends imply that there is a dense molecular packing for systems doped with ionic surfactants as a result of glycerol-surfactant, PVA-surfactant and RhB-surfactant interactions, with overriding importance in SDS-doped films.

Incorporation of cationic surfactants into the plasticised polymer matrix shows the largest variation in sample thickness. CTAB is expected to create wetting layers at both the PVA-air and substrate-PVA interfaces [23], with its excess in the system leading to the formation of surfactant crystals at film-air interface [78]. Compared to the benchmark (composition PVA25), there are no visible morphology changes in the films after addition of CTAB at the investigated concentration, although when both CTAB and RhB were included in the formulation, rod-shaped features appear. These features are also visible for samples containing $C_{12}E_{10}$, however (Fig. 6g and h), hence likely indicate the presence of the tracer.

It is expected that positions with similar diffusivity to the control sample are indicative of similar local composition - i.e. PVA plasticised with glycerol with little to no surfactant present - while areas of high local surfactant concentration will slow down migration of the tracer with resultant slower diffusion coefficient. While migrating through regions with high local concentration of CTAB within the matrix, intermolecular interactions will change migration kinetics and hence tracer diffusivity. For these compositions, similar to solutions doped with SDS, visible phase separation can be observed prior to spin coating, with crystals observed in the solution. While in samples containing SDS they were visible on the preparation day, such crystals could only be observed after ca. 3 days of storage for solutions doped with CTAB, proving weaker CTAB-RhB interactions compared to SDS-RhB interactions, likely due to the steric effects [65].

The average diffusion coefficient of the molecular probe shows the least significant change for the addition of cationic surfactant compared to the control (PVA25 sample). However, bleaching was possible in all tested positions in samples with $C_{12}E_{10}$, contrasting with both SDS and CTAB; furthermore, compositions containing $C_{12}E_{10}$ exhibited morphology that was most similar to benchmark PVA25 sample (Fig. 6e and f). Due to its nonionic nature, $C_{12}E_{10}$ is unlikely to interact with RhB. The higher M_w of $C_{12}E_{10}$ results in overall fewer moles of this substance being present in the system (Table 1) as well as higher entropy penalty connected with its presence on the surface compared to the shorter ionic surfactants [23]. Together with additional factor of glycerol action that is expected to increase compatibility between this surfactant and PVA [23], $C_{12}E_{10}$ is likely the most uniformly-distributed surfactant in the polymer among all three surfactants investigated in the present work. Slower diffusivity of RhB in this system is hence mainly a consequence of steric effects – additional molecules decrease room available for plasticised PVA chain, decreasing its flexibility and diffusion coefficient of fluorescent tracer. Crowding and binding effects for samples doped with surfactants are further indicated by the increase in average fraction of immobile molecules compared to blank sample (Table 2).

3.5. *Modelling fluorophore diffusion in surfactant-doped films*

Due to strong dependence of RhB diffusion coefficient on bleaching position, investigation into mechanism of diffusion would not give reliable results. Therefore, it is assumed that additional intermolecular interactions and crowding effects resulting from surfactant presence would result in diffusion-coupled mechanism. Hence, presented here diffusion coefficient is treated as the effective diffusion coefficient of RhB in these matrices. While fitting FRAP recovery data to the double exponential model, intermolecular interactions influence fast and slow

migrating species, with $\tau_{1/2}$ decreasing according to the affinity of RhB molecule to each surfactant ($\tau_{1/2SDS} > \tau_{1/2CTAB} > \tau_{1/2C12E10}$). Here, the faster species is likely to only interacts with the plasticised polymer backbone rather than surfactants. Less mobile molecules, however, are likely to be dependent on both additional steric effects due to presence of molecules of higher molar mass (nonionic surfactant) or due to ion-ion bonding with migrating tracer (ionic surfactants). Similarly, the more uniform distribution of $C_{12}E_{10}$ introduces the smallest changes in the matrix, while the energetically preferential surface excess of the ionic surfactants leads to lowered uniformity of the film. Interestingly, $\tau_{1/2}$ values for films doped with nonionic or cationic surfactants are either lower or similar to PVA25 composition, indicating that the relative abundance of fast- and slow-moving species changes between formulations, rather than the intrinsic diffusivity of RhB, is responsible for these changes.

As presence of the crystals and surface features may influence the effective diffusion coefficient of the fluorophore in thin films, the additional samples prepared from filtered solutions were investigated and diffusion coefficient therein compared against non-filtered counterparts. The discussion of results obtained for filtered samples without surfactant added is presented in Supporting Information.

The trend of average RhB diffusion coefficient in thin films prepared from filtered solutions (Fig. 5) is similar to that obtained from FCS experiments in solutions of the same compositions [65]. By analysing the range of absolute diffusion coefficient values, no significant difference between samples prepared from filtered and non-filtered solutions appears despite the position-dependence of the diffusion coefficient and lower number of samples investigated for filtered formulations. The notable exceptions are CTAB-doped films where the diffusivity reduces compared to its unfiltered counterpart. This is presumably due to changed solution composition after filtration because of PVA-CTAB-glycerol competitive interactions, leading to decreasing concentration of PVA upon removal of aggregates and consequently amplified steric effects as well as intermolecular interactions. Similar effects were observed upon filtration of PVA25 formulation (Fig. S4 in Supporting Information), indicating that minor changes to solution composition can have large ramifications on film behaviour. For samples containing SDS, however, crystal formation does not lead to substantial differences in diffusion coefficient of RhB, as diffusion coefficient before and after filtration has similar average values and range. Therefore, the differences in diffusion coefficient of RhB in surfactant-doped formulations is caused by intermolecular interactions and steric effects rather than precipitation observed.

4. Conclusions

Investigations of molecular probe diffusion were performed on PVA thin films, where diffusion can be approximated as lateral. Diffusion characteristics of RhB were found to be dependent on the presence of glycerol (plasticiser) and chemistry of any added surfactant (cationic/anionic/nonionic). Different diffusion kinetics were observed in thin films of various PVA/glycerol ratio - tracer diffusion coefficient increased with increasing glycerol concentration at concentrations below the compatibility limit of ca. 40 wt%, whereupon it decreased below the diffusion rate of unplasticized PVA. Above the PVA/glycerol compatibility limit, further increase in plasticiser concentration resulted in glycerol aggregation and consequent phase separation on microscale which inhibited the probe molecule from migrating freely.

Addition of any surfactant (at ca. 6 wt%) hindered the diffusion coefficient of RhB by 30 %, 61 % and 88 % for cationic, nonionic and anionic surfactant compared to control sample, respectively. Steric effects due to the presence of guest molecules of higher M_w in the system seem to explain those phenomena in compositions containing the nonionic surfactant. However, for films with cationic or anionic surfactant, it is likely that surfactant-fluorophore interactions play a main role, slowing down the diffusion of the RhB.

This data shows the influence of the system chemistry on diffusive properties of real-life products and provides an initial set of design rules that need to be considered while trying to minimise the aging phenomena therein. We show that it is possible to identify these phenomena by measuring changes in the diffusion characteristics within the given system caused by changes in formulation composition (e.g. local phase separation above PVA/glycerol compatibility limit). These results should now be extended to show how migration of contaminants such as surfactants is changed by variation in storage environmental conditions.

CRediT authorship contribution statement

Katarzyna Majerczak: Conceptualization, Methodology, Validation, Formal analysis, Investigation, Data Curation, Writing – Original Draft; **Zhiwei Shi**: Conceptualization, Validation, Writing – Review and Editing; **Zhanping Zhang**: Conceptualization, Validation, Writing – Review and Editing; **Zhenyu Jason Zhang**: Conceptualization, Methodology, Validation, Writing – Review and Editing, Visualization, Supervision, Project administration, and Funding acquisition.

Declaration of competing interest

The authors declare that they have no known competing financial interests or personal relationships that could have appeared to influence the work reported in this paper.

Data availability

Data will be made available on request.

Acknowledgements

This research was funded by School of Chemical Engineering, University of Birmingham, and Engineering & Physical Science Research Council (EPSRC) with grant number EP/P007864/1. ZJZ acknowledges an Industrial Fellowship with P&G, funded by the Royal Academy of Engineering (IF2021\100).

Appendix A. Supplementary data

Supplementary data to this article can be found online at https://doi.org/10.1016/j.porgcoat.2023.107833.

References

[1] J.N. Hahladakis, C.A. Velis, R. Weber, E. Iacovidou, P. Purnell, An overview of chemical additives present in plastics: migration, release, fate and environmental impact during their use, disposal and recycling, J. Hazard. Mater. 344 (2018) 179–199.
[2] W.A.C. Anderson, L. Castle, Benzophenone in cartonboard packaging materials and the factors that influence its migration into food, Food Addit. Contam. 20 (2003) 607–618.
[3] M. Sharman, C.A. Honeybone, S.M. Jickells, L. Castle, Detection of residues of the epoxy adhesive component bisphenol a diglycidyl ether (BADGE) in microwave susceptors and its migration into food, Food Addit. Contam. 12 (1995) 779–787.
[4] C. Smaranda, M. Gavrilescu, Migration and fate of persistent organic pollutants in the atmosphere - a modelling approach, Environ. Eng. Manag. J. 7 (2008) 743–761.
[5] H. Lee, L.A. Archer, Functionalizing polymer surfaces by surface migration of copolymer additives: role of additive molecular weight, Polymer (Guildf). 43 (2002) 2721–2728.
[6] T.C. Chan, H.T. Li, K.Y. Li, Effects of shapes of solute molecules on diffusion: a study of dependences on solute size, solvent, and temperature, J. Phys. Chem. B 119 (2015) 15718–15728.
[7] A. Reynier, P. Dole, S. Humbel, A. Feigenbaum, Diffusion coefficients of additives in polymers. I. Correlation with geometric parameters, J. Appl. Polym. Sci. 82 (2001) 2422–2433.
[8] G. Wypych, 8. Effect of Plasticizers On Other Components of Formulations, 2017.
[9] V. Senichev, V. Tereshatov, G. Wypych, Handbook of Plasticizers, William Andrew Publishing, Boston, 2012, pp. 135–164.
[10] A. F, I.-H. B, T. H, Migration of additives in rubber, Gummi Fasern Kunststoffe (2004) 653–662.

[11] E.F.D. Sabattié, J. Tasche, M.R. Wilson, M.W.A. Skoda, A. Hughes, T. Lindner, R. L. Thompson, Predicting oligomer/polymer compatibility and the impact on nanoscale segregation in thin films, Soft Matter 13 (2017) 3580–3591.
[12] G. Wypych, Handbook of Plasticizers, William Andrew Publishing, Boston, 2012, pp. 165–185.
[13] M. Hesami, W. Steffen, H.-J.J. Butt, G. Floudas, K. Koynov, Molecular probe diffusion in thin polymer films: evidence for a layer with enhanced mobility far above the glass temperature, ACS Macro Lett. 7 (2018) 425–430.
[14] C. Hubert, E. Malcor, I. Maurin, J.M. Nunzi, P. Raimond, C. Fiorini, Microstructuring of polymers using a light-controlled molecular migration processes, Appl. Surf. Sci. 186 (2002) 29–33.
[15] J. Krawczyk, S. Croce, T.C.B. McLeish, B. Chakrabarti, Elasticity dominated surface segregation of small molecules in polymer mixtures, Phys. Rev. Lett. 116 (2016), 208301.
[16] P.J. Flory, Thermodynamics of high polymer solutions, J. Chem. Phys. 10 (1942) 51–61.
[17] M.L. Huggins, Solutions of long chain compounds, J. Chem. Phys. 9 (1941) 440.
[18] V.R. Gundabala, W.B. Zimmerman, A.F. Routh, A model for surfactant distribution in latex coatings, Langmuir 20 (2004) 8721–8727.
[19] A. Gromer, F. Thalmann, P. Hébraud, Y. Holl, Simulation of vertical surfactant distributions in drying latex films, Langmuir 33 (2017) 561–572.
[20] R.A. Campbell, K.J. Edler, Growth-collapse mechanism of PEI-CTAB films at the air-water interface, Soft Matter 7 (2011) 11125–11132.
[21] K.J. Edler, M.J. Wasbrough, J.A. Holdaway, B.M.D. O'Driscoll, Self-assembled films formed at the air - water interface from CTAB/SDS mixtures with water-soluble polymers, Langmuir 25 (2009) 4047–4055.
[22] A. Briddick, R.J. Fong, E.F.D. Sabattié, P. Li, M.W.A. Skoda, F. Courchay, R. L. Thompson, Blooming of smectic surfactant/plasticizer layers on spin-cast poly (vinyl alcohol) films, Langmuir 34 (2018) 1410–1418.
[23] A. Briddick, P. Li, A. Hughes, F. Courchay, A. Martinez, R.L. Thompson, Surfactant and plasticizer segregation in thin poly(vinyl alcohol) films, Langmuir 32 (2016) 864–872.
[24] G. Wypych, Handbook of Plasticizers, William Andrew Publishing, Boston, 2012, pp. 563–571.
[25] K.K. Senanayake, E.A. Fakhrabadi, M.W. Liberatore, A. Mukhopadhyay, Diffusion of nanoparticles in entangled poly(vinyl alcohol) solutions and gels, Macromolecules 52 (2019) 787–795.
[26] T. Cherdhirankorn, V. Harmandaris, A. Juhari, P. Voudouris, G. Fytas, K. Kremer, K. Koynov, Fluorescence correlation spectroscopy study of molecular probe diffusion in polymer melts, Macromolecules 42 (2009) 4858–4866.
[27] A. Budkowski, Interfacial phenomena in thin polymer films: phase coexistence and segregation: interfaces crystallization viscoelasticity, Adv. Polym. Sci. 148 (1999) 1–111.
[28] M. Geoghegan, G. Krausch, Wetting at polymer surfaces and interfaces, Prog. Polym. Sci. 28 (2003) 261–302.
[29] M.F. Poças, J.C. Oliveira, F.A.R. Oliveira, T. Hogg, A critical survey of predictive mathematical models for migration from packaging, Crit. Rev. Food Sci. Nutr. 48 (2008) 913–928.
[30] A. O'Brien, A. Goodson, I. Cooper, Polymer additive migration to foods - a direct comparison of experimental data and values calculated from migration models for high density polyethylene (HDPE), Food Addit. Contam. 16 (1999) 367–380.
[31] A. O'Brien, I. Cooper, Polymer additive migration to foods - a direct comparison of experimental data and values calculated from migration models for polypropylene, Food Addit. Contam. 18 (2001) 343–355.
[32] T. Begley, L. Castle, A. Feigenbaum, R. Franz, K. Hinrichs, T. Lickly, P. Mercea, M. Milana, A. O'Brien, S. Rebre, R. Rijk, O. Piringer, Evaluation of migration models that might be used in support of regulations for food-contact plastics, Food Addit. Contam. 22 (2005) 73–90.
[33] I.S. Arvanitoyannis, L. Bosnea, Migration of substances from food packaging materials to foods, Crit. Rev. Food Sci. Nutr. 44 (2004) 63–76.
[34] S. Zhu, N. Welsh, D.E. Hirt, Determination of the diffusivity of a hydrophilic migratory additive in Ipp films, J. Plast. Film Sheeting 23 (2007) 187–201.
[35] E. Van Keuren, W. Schrof, Fluorescence recovery after two-photon bleaching for the study of dye diffusion in polymer systems, Macromolecules 36 (2003) 5002–5007.
[36] W. Schrof, J. Klingler, S. Rozouvan, D. Horn, Raman correlation spectroscopy: a method for studying chemical composition and dynamics of disperse systems, Phys. Rev. E - Stat. Physics, Plasmas, Fluids, Relat. Interdiscip. Top. 57 (1998) R2523–R2526.
[37] H. Vural, J. Maisch, I. Gerhardt, M. Jetter, S.L. Portalupi, P. Michler, Characterization of spectral diffusion by slow-light photon-correlation spectroscopy, Phys. Rev. B 101 (2020) 1–6.
[38] D. Wöll, Fluorescence correlation spectroscopy in polymer science, RSC Adv. 4 (2014) 2447–2465.
[39] M. Mears, Z.J. Zhang, R.C.D. Jackson, Y. Si, T.J.B. Bradford, J.M. Torkelson, M. Geoghegan, Lateral diffusion of single poly(ethylene oxide) chains on the surfaces of glassy and molten polymer films, J. Chem. Phys. 154 (2021), 164902.
[40] Z.J. Zhang, J. Madsen, N.J. Warren, M. Mears, G.J. Leggett, A.L. Lewis, M. Geoghegan, Influence of salt on the solution dynamics of a phosphorylcholine-based polyzwitterion, Eur. Polym. J. 87 (2017) 449–457.
[41] P.J. McDonald, J. Godward, R. Sackin, R.P. Sear, Surface flux limited diffusion of solvent into polymer, Macromolecules 34 (2001) 1048–1057.
[42] D.M. Lane, P.J. McDonald, The visualization of spatial gradients in polymer and solvent dynamics for mixed solvents ingressing poly(methyl methacrylate) using stray field magnetic resonance imaging, Polymer (Guildf). 38 (1997) 2329–2335.
[43] B.A. Kowert, N.C. Dang, K.T. Sobush, L.G. Seele, Diffusion of aromatic hydrocarbons in n-alkanes and cyclohexanes, J. Phys. Chem. A 105 (2001) 1232–1237.
[44] F.P. Duval, P. Porion, H. Van Damme, Microscale and macroscale diffusion of water in colloidal gels. A pulsed field gradient and NMR imaging investigation, J. Phys. Chem. B 103 (1999) 5730–5735.
[45] A. Veniaminov, T. Jahr, H. Sillescu, E. Bartsch, Length scale dependent probe diffusion in drying acrylate latex films, Macromolecules 35 (2002) 808–819.
[46] T.P. Gall, E.J. Kramer, Diffusion of deuterated toluene in polystyrene, Polymer (Guildf). 32 (1991) 265–271.
[47] T.P. Gall, R.C. Lasky, E.J. Kramer, Case II diffusion: effect of solvent molecule size, Polymer (Guildf). 31 (1990) 1491–1499.
[48] S. Seiffert, W. Opperman, Systematic evaluation of FRAP experiments performed in a confocal laser scanning microscope, J. Microsc. 220 (2005) 20–30.
[49] P. Jönsson, M.P. Jonsson, J.O. Tegenfeldt, F. Höök, A method improving the accuracy of fluorescence recovery after photobleaching analysis, Biophys. J. 95 (2008) 5334–5348.
[50] B. Frank, A.P. Gast, T.P. Russell, H.R. Brown, C. Hawker, Polymer mobility in thin films, Macromolecules 29 (1996) 6531–6534.
[51] L. Jourdainne, S. Lecuyer, Y. Arntz, C. Picart, P. Schaaf, B. Senger, J.-C. Voegel, P. Lavalle, T. Charitat, Dynamics of poly(l-lysine) in hyaluronic acid/poly(l-lysine) multilayer films studied by fluorescence recovery after pattern Photobleaching, Langmuir 24 (2008) 7842–7847.
[52] D. Raz-Ben Aroush, N. Ofer, E. Abu-Shah, J. Allard, O. Krichevsky, A. Mogilner, K. Keren, Actin turnover in lamellipodial fragments, Curr. Biol. 27 (2017) 2963–2973.
[53] S. Merouani, O. Hamdaoui, F. Saoudi, M. Chiha, Sonochemical degradation of rhodamine B in aqueous phase: effects of additives, Chem. Eng. J. 158 (2010) 550–557.
[54] I.L. Arbeloa, P.R. Ojeda, Molecular forms of rhodamine B, Chem. Phys. Lett. 79 (1981) 347–350.
[55] E.T. Soares, M.A. Lansarin, C.C. Moro, A study of process variables for the photocatalytic degradation of rhodamine B, Braz. J. Chem. Eng. 24 (2007) 29–36.
[56] N.O. Mchedlov-Petrossyan, N.A. Vodolazkaya, A.O. Doroshenko, Ionic equilibria of fluorophores in organized solutions: the influence of micellar microenvironment on protolytic and photophysical properties of rhodamine B, J. Fluoresc. 13 (2003) 235–248.
[57] E. Van Keuren, W. Schrof, Two-photon pattern bleaching for characterizing structural changes in polymer films, Macromol. Rapid Commun. 23 (2002) 1138–1140.
[58] S. Seiffert, W. Oppermann, Diffusion of linear macromolecules and spherical particles in semidilute polymer solutions and polymer networks, Polymer (Guildf). 49 (2008) 4115–4126.
[59] Z. Zhang, M. Moxey, A. Alswieleh, A.J. Morse, A.L. Lewis, M. Geoghegan, G. J. Leggett, Effect of salt on phosphorylcholine-based zwitterionic polymer brushes, Langmuir 32 (2016) 5048–5057.
[60] M. Kang, C.A. Day, A.K. Kenworthy, E. DiBenedetto, Simplified equation to extract diffusion coefficients from confocal FRAP data, Traffic 13 (2012) 1589–1600.
[61] R.J. Fong, A. Robertson, P.E. Mallon, R. L., Thompson, polymers the impact of plasticizer and degree of hydrolysis on free volume of poly (vinyl alcohol), Films (2018) 1–15.
[62] R.J. Fong, A. Robertson, P.E. Mallon, R.L. Thompson, The impact of plasticizer and degree of hydrolysis on free volume of poly(vinyl alcohol) films, Polymers (Basel) 10 (2018) 1036.
[63] Z. Fu, Y. Yao, S. Guo, K. Wang, Q. Zhang, Q. Fu, Effect of plasticization on stretching stability of poly(vinyl alcohol) films: a case study using glycerol and water, Macromol. Rapid Commun. 44 (2023) 2200296.
[64] K. Majerczak, J.R.H. Manning, Z. Shi, Z. Zhang, Z.J. Zhang, Surface wetting kinetics of water soluble organic film, Prog. Org. Coat. 177 (2023), 107436.
[65] K. Majerczak, O. Squillace, Z. Shi, Z. Zhang and Z. J. Zhang, Molecular diffusion in ternary poly(vinyl alcohol) solutions, Front. Chem. Sci. Eng.
[66] R.A.L. Jones, The dynamics of thin polymer films, Curr. Opin. Colloid Interface Sci. 4 (1999) 153–158.
[67] A. Bansal, H. Yang, C. Li, K. Cho, B.C. Benicewicz, S.K. Kumar, L.S. Schadler, Quantitative equivalence between polymer nanocomposites and thin polymer films, Nat. Mater. 4 (2005) 693–698.
[68] T. Karbowiak, H. Hervet, L. Léger, D. Champion, F. Debeaufort, A. Voilley, Effect of plasticizers (water and glycerol) on the diffusion of a small molecule in iota-carrageenan biopolymer films for edible coating application, Biomacromolecules 7 (2006) 2011–2019.
[69] J. Jang, D.K. Lee, Plasticizer effect on the melting and crystallization behavior of polyvinyl alcohol, Polymer (Guildf). 44 (2003) 8139–8146.
[70] B. Sprague, J. McNally, FRAP analysis of binding: proper and fitting, Trends Cell Biol. 15 (2005) 84–91.
[71] D.A. Stavreva, J.G. McNally, Fluorescence recovery after photobleaching (FRAP) methods for visualizing protein dynamics in living mammalian cell nuclei, Methods Enzymol. 375 (2003) 443–455.
[72] B.L. Sprague, R.L. Pego, D.A. Stavreva, J.G. McNally, Analysis of binding reactions by fluorescence recovery after photobleaching, Biophys. J. 86 (2004) 3473–3495.
[73] P. Chang, J. Torres, R.A. Lewis, K.L. Mowry, E. Houliston, M. Lou King, Localization of RNAs to the mitochondrial cloud in Xenopus oocytes through entrapment and association with endoplasmic reticulum, Mol. Biol. Cell 15 (2004) 4669–4681.
[74] Y. Sakai, M. Kawahigashi, T. Minami, T. Inoue, S. Hirayama, Deconvolution of non-exponential emission decays arising from reabsorption of emitted light, J. Lumin. 42 (1989) 317–324.

[75] B.O. Haglund, L.-O. Sundelöf, S.M. Upadrashta, D.E. Wurster, Effect of SDS micelles on rhodamine-B diffusion in hydrogels, J. Chem. Educ. 73 (1996) 889.
[76] H. Tajalli, A. Ghanadzadeh Gilani, M.S. Zakerhamidi, M. Moghadam, Effects of surfactants on the molecular aggregation of rhodamine dyes in aqueous solutions, Spectrochim. Acta Part A Mol. Biomol. Spectrosc. 72 (2009) 697–702.
[77] L.-X.X. Yang, Y.-J.J. Zhu, H. Tong, W.-W.W. Wang, Submicrocubes and highly oriented assemblies of MnCO3 synthesized by ultrasound agitation method and their thermal transformation to nanoporous Mn2O3, Ultrason. Sonochem. 14 (2007) 259–265.
[78] K. Majerczak, Z. Shi, Z. Zhang and Z. Zhang, Humidity- and surfactant-accelerated aging of molecular thin films, Prep.